

Analysis of the Adaptive Threshold Vehicle Detection Algorithm Applied to Traffic Vibrations

Roland Hostettler and Wolfgang Birk

This is a post-print of a paper published in *18th IFAC World Congress*. When citing this work, you must always cite the original article:

Hostettler, R. and Birk, W. (2011). Analysis of the adaptive threshold vehicle detection algorithm applied to traffic vibrations. In *18th IFAC World Congress*. Milano, Italy

DOI:

n/a

Copyright:

© 2016 IFAC. This is the author's version of a work that was accepted for publication in ifac-papersonline.net. Changes resulting from the publishing process, such as peer review, editing, corrections, structural formatting, and other quality control mechanisms may not be reflected in this document. Changes may have been made to this work since it was submitted for publication. A definitive version was subsequently published in ifac-papersonline.net.

Analysis of the Adaptive Threshold Vehicle Detection Algorithm Applied to Traffic Vibrations^{*}

Roland Hostettler^{*} Wolfgang Birk^{*}

^{*} *Luleå University of Technology, Division of Systems and Interaction,
971 87 Luleå, Sweden (e-mail: {rolhos,wolfgang}@ltu.se).*

Abstract: This paper discusses and analyzes the performance of the Adaptive Threshold Detection Algorithm for vehicle detection based on road traffic vibrations. The algorithm, originally developed for magnetometer- and microphone-based vehicle detection, is adapted for the usage with seismic signals and then analyzed in a statistical framework. It is found that the algorithm can be applied to this kind of signals and promising results are obtained in simulations and tests on measurement data. Further testing using real traffic data is required in order to obtain more significant results.

Keywords: Accelerometers, Algorithms, Detection Algorithms, Detector Performance Analysis

1. INTRODUCTION

Due to the advances in electronics and sensor systems, many novel traffic detectors have been developed in recent years. Besides high-end solutions, for example video or radar which are used scarcely, low cost sensors such as microphones or magnetometers are widely considered as a replacement for the somewhat outdated detectors such as inductive loops or pressure tubes that are currently used (Sullivan et al., 2005; Honeywell, 2005). Furthermore, small low cost sensors can be used much more widely which will enable novel applications in infrastructure-to-infrastructure or vehicle-to-infrastructure scenarios in the future (see, e.g. Birk et al. (2009)).

Magnetometers were first perceived as a direct replacement for inductive loops. Both are based on similar phenomena and provide similar information. Vehicle detection has been investigated by Cheung and Varaiya (2007) who proposed the Adaptive Threshold Detection Algorithm (ATDA) for different sensing sources such as magnetometers or microphones. The ATDA is a simplistic, yet presumably reliable detection algorithm as it has been shown experimentally by Ding et al. (2004). Commercial vehicle detector products based on magnetometers are available and in use nowadays (SENSYS Networks, 2010). Recent research has taken magnetometer-based sensing even further and, for example, vehicle velocity can be estimated and vehicles can even be tracked using magnetometers (Isaksson, 2008; Wahlström et al., 2010).

Another approach was introduced by Hostettler et al. (2010) where the seismic signal on the road surface is measured in order to estimate vehicle parameters. This is more seen as an approach comparable to pressure tubes since the measured signal is caused by the vehicle-ground

interaction and it is expected that additional vehicle-related parameters such as axle load can be estimated using this method. In any of the schemes there arises the elementary question of what performance a vehicle detector can achieve. Therefore, it is the objective of this paper to analyze the performance of the above mentioned Adaptive Threshold Detection Algorithm using the seismic signals measured by an accelerometer instead of a magnetometer or microphone as an input. Since the algorithm has only been verified experimentally, we will first analyze it in terms of a statistical framework and assess the theoretical performance. The algorithm is then applied to traffic vibrations in order to verify the previous results.

The organization of the paper is as follows. First, the signal model for seismic signals is presented in Section 2. Then, the algorithm is introduced and described in Section 3. In Section 4, the statistical properties, timing constraints and parameters are discussed. The analysis is followed by a simulation using the introduced signal- and disturbance models as well as using real traffic vibration data in Section 5. Concluding remarks are given in Section 6.

2. SIGNAL MODEL

Unlike other phenomena such as magnetics, road traffic vibrations and propagation have not been understood to the same degree. Different approaches such as using random characterization or tire-pavement interaction modelling have been studied (Hunt, 1991; Sun and Kennedy, 2002; Hao and Ang, 1998). Nevertheless, based on previous observations (Hostettler et al., 2010) we identify the following two hypotheses

$$H_0 : x^{(0)}[n] = e[n] \quad (1)$$

$$H_1 : x^{(1)}[n] = s[n] + e[n] \quad (2)$$

^{*} Financial support from *Gunnar och Märtha Bergendahls Stiftelse*, GEVEKO AB and the Swedish Governmental Agency for Innovation Systems (VINNOVA) are hereby gratefully acknowledged.

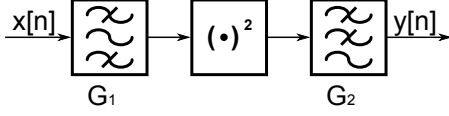


Fig. 1. Traffic vibration pre-processing: The measured seismic signal is first band-limited and then the signal envelope is estimated using a square-law device followed by a low-pass filter.

where the bracketed superscript denotes the respective hypothesis (H_0 or H_1).

In the first case, denoted H_0 , only sensor noise is measured, i.e. no vehicle passes. It is assumed that $e[n] \sim \mathcal{N}(0, \sigma^2)$ is additive white Gaussian noise. For H_1 , the signal includes not only noise but also a band-limited vibration component $s[n]$ and additive noise $e[n]$ as described before. $s[n]$ is approximated by an exponentially pulsed harmonic vibration

$$s[n] = Ap[n] \cos(\omega_0 n) = Ae^{-(\omega_b n)^2} \cos(\omega_0 n) \quad (3)$$

where ω_b is the pulse bandwidth and ω_0 the center frequency (normalized frequencies in *radians/sample*). We note that $s[n]$ denotes the vibrations caused by one axle. This implies that a vehicle with multiple axles causes a superposition of multiple pulses $s[n]$.

3. ALGORITHM DESCRIPTION

The detection scheme proposed by Cheung and Varaiya (2007) foresees a two-stage processing of the source signal where the signal first is pre-processed and then used in the name-giving ATD algorithm. Clearly, it is the first of these two stages which depends on the source signal used whereas the second stage remains the same.

3.1 Pre-processing

The pre-processing applied to the vibration signal is a chain consisting of a pre-filter, squarer and post-filter as depicted in Fig. 1.

The pre-filter G_1 is a band-pass filter that limits the signal to the desired range. The corner frequencies for G_1 are ω_l and ω_u and they enclose the seismic signal caused by a vehicle as described in Section 2. The post-filter G_2 is a low-pass filter with cut-off frequency ω_c that regains the envelope pulse $p[n]$. Analysis of the pre-processing stage is done assuming ideal filters. Practical tests showed that elliptical filters with corner frequencies $\omega_l = 0.5\pi$, $\omega_u = 0.77\pi$ and order $N_{G_1} = 12$ for the pre-filter G_1 and cut-off frequency $\omega_c = 0.009\pi$ and order $N_{G_2} = 7$ for the post-filter G_2 satisfy this assumption. The filter frequency responses are therefore given by

$$G_1(\omega) = \text{rect}\left(\frac{\omega}{2\omega_u}\right) - \text{rect}\left(\frac{\omega}{2\omega_l}\right) \quad (4)$$

$$G_2(\omega) = \text{rect}\left(\frac{\omega}{2\omega_c}\right) \quad (5)$$

where

Table 1. Adaptive Threshold Detection Algorithm (ATDA) detector summary.

1.	If $v[n] = 0$ and $\sum_{k=0}^{N_s-1} d[n-k] = 0$ $b[n] = (1 - \alpha)b[n-1] + \alpha y[n]$ else $b[n] = b[n-1]$
2.	$z[n] = y[n] - b[n]$
3.	If $z[n] \geq T$ $v[n] = 1$ else $v[n] = 0$
4.	$B_1[n] = \sum_{k=0}^{N_1-1} v[n-k]$ $B_2[n] = \sum_{k=0}^{N_0-1} v[n-k]$
5.	If $B_1[n] = N_1$ and $d[n-1] = 0$ $d[n] = 1$ else if $B_2[n] = 0$ and $d[n-1] = 1$ $d[n] = 0$ else $d[n] = d[n-1]$

$$\text{rect}(x) = \begin{cases} 1 & |x| \leq 1/2 \\ 0 & \text{otherwise} \end{cases}.$$

It should also be noted that this pre-processing can be seen as an envelope demodulator. The resulting signal is the input to the detector described next.

3.2 Detection

The actual detector is summarized in Table 1. First, a so called adaptive base-line compensation is performed. This is in effect a high-pass filter that removes possible offsets from the pre-processed signal. In the case of magnetometers, it is known that the offset is temperature dependent (Cheung and Varaiya, 2007). The base-line compensation's effect on the vibration signal is analyzed in Section 4.2. The output $z[n]$ is the difference between the base-line $b[n]$ and the input $y[n]$:

$$z[n] = y[n] - b[n] \quad (6)$$

where

$$b[n] = \begin{cases} (1 - \alpha)b[n-1] + \alpha y[n] & v[n] + \sum_{k=0}^{N_s-1} d[n-k] = 0 \\ b[n-1] & \text{otherwise} \end{cases} \quad (7)$$

α determines the convergence rate, $v[n]$ is the thresholded signal $z[n]$ as given by (8), and $d[n]$ is the detection flag (see below). From (7) we note that the base-line is only adapted when H_0 is measured.

$z[n]$ is then compared to a predefined threshold T yielding

$$v[n] = \begin{cases} 1 & z[n] \geq T \\ 0 & z[n] < T \end{cases} \quad (8)$$

Then, it is evaluated for how long $v[n]$ remains stable. The two counters $B_1[n]$ and $B_2[n]$ calculate the sum of the last N_1 and N_0 samples of $v[n]$.

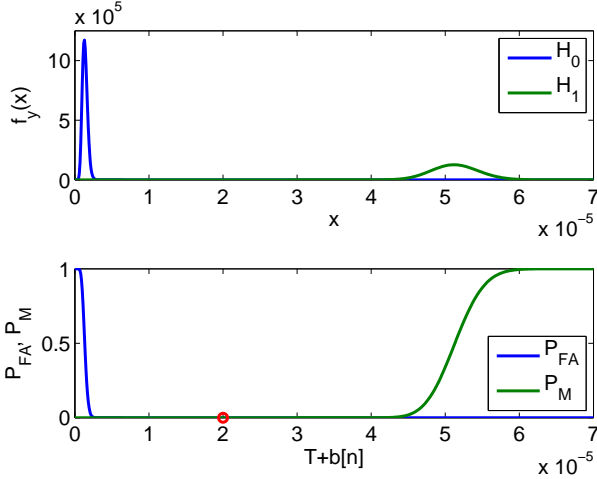


Fig. 2. Probability density functions $f_y(x)$ for the two hypotheses H_0 and H_1 (top) and trade-off curves for the probabilities of false positives and false negatives (bottom). The circle marks the chosen value at $T + b[n] = 2 \cdot 10^{-5}$.

$$B_1[n] = \sum_{k=0}^{N_1-1} v[n-k] \quad (9)$$

$$B_2[n] = \sum_{k=0}^{N_0-1} v[n-k] \quad (10)$$

From these counters the final decision whether a vehicle has passed or not is taken as follows:

- (1) If $B_1[n] = N_1$ and $d[n-1] = 0$ a new vehicle is detected and hence $d[n] = 1$.
- (2) If $B_2[n] = 0$ and $d[n-1] = 1$ the vehicle has passed the sensor completely and hence $d[n] = 0$.
- (3) In any other case, the previous state is retained, i.e. $d[n] = d[n-1]$.

A vehicle is detected whenever $d[n] = 1$.

4. ANALYSIS

4.1 Preprocessing

The signal properties for $y[n]$ based on the hypotheses given in (1) and (2) are derived in Appendix A. Here only the main results are used for further analysis.

Typical values for high sensitivity accelerometers are $\sigma^2 = 5 \cdot 10^{-6} (m/s^2)^2$ and experiments have shown that a car passing at a distance of $d = 1m$ has a minimal amplitude of $A = 0.01m/s^2$. Using these values, Fig. 2 shows the Γ -distributions for the two cases. It is obvious that excellent detection results can be obtained with such a sensor since the distributions are well separated due to the high signal to noise ratio.

4.2 Adaptive Base-Line

As described in Section 3 the adaptive base-line is calculated depending on the N_S past states (see Eq. (7)). This implies that if T is exceeded by $z[n]$, $b[n]$ is not adapted

and the previous value is retained. That in turn means that the base-line is adapted if and only if H_0 is measured. The expected value of $b[n]$ is therefore given by

$$E\{b[n]\} = E\left\{(1-\alpha)b[n-1] + \alpha y^{(0)}[n]\right\} = \eta_y^{(0)}, \quad (11)$$

i.e. it converges to the (pre-processed) noise mean. Thus, for the signal given, the base-line compensation shifts the pre-processed signal by $\eta_y^{(0)}$. This is in agreement with the offset-removing function as identified in Section 3.2.

4.3 Threshold

Depending on the application, different design goals are of importance when determining a detection threshold, e.g. the cost for a false positive might be much higher than the cost for a false negative and therefore the threshold is chosen in order to minimize the false positives. In the present application, no cost is assigned to neither of the false detections. Therefore, a threshold for equal probabilities of miss (P_M) and false alarm (P_{FA}) is desired. P_{FA} is given as

$$P_{FA} = P(z[n] \geq T | H_0) = 1 - P(y[n] < T + b[n] | H_0) \quad (12)$$

and P_M as

$$P_M = P(z[n] < T | H_1) = P(y[n] < T + b[n] | H_1). \quad (13)$$

Fig. 2 shows the curves for $P_{FA} = 1 - P(T + b[n] | H_0)$ and $P_M = P(T + b[n] | H_1)$. The intersection of the two curves is the sought value as described above. As expected from Section 4.1, the strong signal to noise ratio makes it possible to choose a point where P_M and P_{FA} reach virtually zero. It is noted that the separation of the error rate curves shown in Fig. 2 becomes less for worse noise figures, e.g. for cheaper integrated sensors, which in turn leads to worse performance characteristics.

4.4 Timing Considerations and Constraints

The parameters N_1 and N_0 affect the algorithms responsiveness to detection and recovery. N_1 essentially defines the time the sensor has to be occupied by a target for the algorithm to detect it as a target. This has the effect that short disturbances of length $< N_1$ are rejected and the threshold has to be exceeded by the vehicle for at least N_1 samples. If N_1 is chosen too large, the rate of false negatives is increased but at the same time stronger disturbances can be rejected. N_1 also introduces a delay between the time when the vehicles actually arrives at the sensor and the time it is detected. In the U.S. this delay is required to not exceed $100ms$ (Federal Highway Administration, 2006, pp. J-1ff.).

The time N_0 on the other hand is a means to reject negative disturbances. If due to some reason the input signal falls below the threshold for a short time that is smaller than N_0 , it is assumed that this is a disturbance. Only if the signal drops below the threshold permanently (i.e. for a time longer than N_0), new vehicles can be

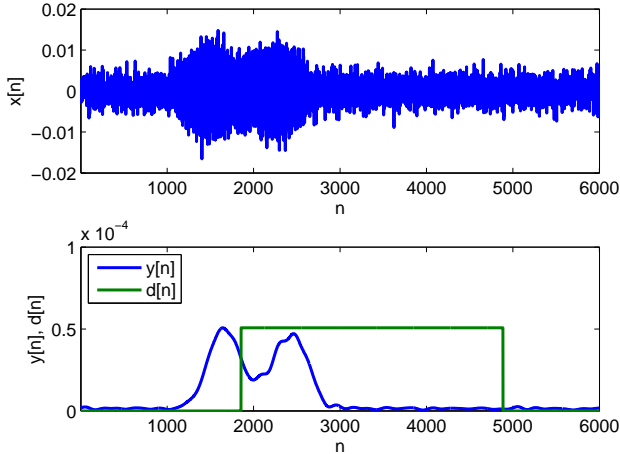


Fig. 3. Example of a simulated signal. The modelled signal according to Section 2 (top) and the pre-processed signal together with the detection window (bottom).

Table 2. Algorithm parameters used for simulation and logged data.

Parameter	Value
α	$1 \cdot 10^{-6}$
T	$1.86 \cdot 10^{-5}$
N_1	440 ($\triangleq 0.1s$)
N_0	2200 ($\triangleq 0.5s$)

Table 3. Algorithm results for the simulation and real data.

	Simulation	Sensor 1	Sensor 2
No. of Vehicles	1000	142	142
Detected	1000	142	142
Missed	0	0	0
False Alarm	0	0	1

detected. This has as a side effect that vehicles following each other very tightly might be counted as one, yielding a false negative error. The choice of N_0 can therefore be linked to driver behavior and performance such as a driver's choice of the distance to the next vehicle and driver reaction times (Triggs and Harris, 1982).

5. RESULTS AND DISCUSSION

5.1 Simulation

Different cases are simulated here in order to illustrate the algorithm performance as analyzed. First, the ideal case is considered where vehicles follow each other with an inter-vehicle distance of more than 1s. Fig. 3 shows this kind of signal as described in Section 2. $N_{sim} = 1000$ samples of this type with signal and noise characteristics as described before and algorithm parameters as shown in Table 2 were simulated. This yielded no errors as expected and the results are listed in Table 3.

Another simulation was run to verify the timing constraints regarding N_0 in order to verify miss in cases where two vehicles are following very closely. Table 4 shows the

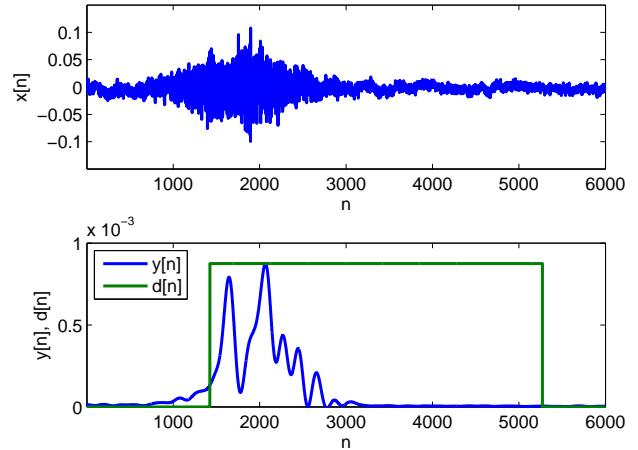


Fig. 4. Traffic vibrations for a passenger car. The measured vibration signal on top and the pre-processed signal together with the detection below.

Table 4. Results for the simulation where two cars follow each other very tightly for different values of Δt .

Δt	0.25s	0.5s	1s
No. of Simulations	1000	1000	1000
No. of Vehicles	2000	2000	2000
Detected	1000	1000	2000
Missed	1000	1000	0
False Alarm	0	0	0

results for simulations with an inter-vehicle spacing of $\Delta t = 0.25s$, $\Delta t = 0.5s$, and $\Delta t = 1s$ with $N_{sim} = 1000$ simulations per value of Δt .

5.2 Traffic Vibration Data

The algorithm was also applied to road vibrations measured as described by Hostettler et al. (2010). In these experiments, 142 vehicle signatures were measured with two spatially separated accelerometers. The signatures include a broad variety of vehicles: passenger cars, passenger cars with trailers, delivery trucks, trucks and trucks with trailers. Fig. 4 shows a typical signal for a passenger car together with the envelope and the window where a vehicle occupies the sensor.

The results from applying the algorithm to this data are also given in Table 3. As expected, all the vehicles are detected for both sensors. However, for sensor 2, there is one false alarm that was triggered. Analysis of that specific case showed that this is due to a strong pulse-like disturbance that was not rejected.

5.3 Discussion

The simulations as well as the results from applying the algorithm confirms the analysis developed in Section 4 and the detection performance was very good.

However, a weakness in the disturbance rejection of the algorithm was revealed. A false detection was triggered due to a strong pulse of unknown origin. It can be assumed that

such disturbances are quite common in seismic signals, e.g. due to nearby construction work or percussive drilling. The algorithm could not resolve that problem which indicates that future work has to address this kind of problem more thoroughly.

Some more thought is now given to the choice of the parameters. Except for the detection threshold, these were chosen manually, based on assumptions made on how drivers behave and on limits specified by authorities. Another more robust option to determine the parameters is, for example, the use of Monte Carlo simulations where parameters are chosen based on a predefined optimality criterion (see, e.g. Andrieu et al. (2003)). This certainly yields a more reliable choice of parameters and should be considered for further development.

6. CONCLUSION

In this paper, the Adaptive Threshold Detection Algorithm as proposed by Cheung and Varaiya (2007) has been described and analyzed in detail. It has been shown that the algorithm, originally intended for vehicle detection using magnetometers and microphones, can be applied to road vibrations measured by accelerometers.

The algorithm's performance has been analyzed in terms of signal statistics and it was shown that very good signal and noise separation can be achieved which yields high detection rates. Data from simulations and real-life experiments were tested on the algorithm and confirmed the theoretical analysis.

Despite the good results, some additional remarks should be made. First, the assumed signal model is appropriate for this analysis, does, however, not reflect the complex physics involved in traffic vibrations and might prove wrong for other applications. Finally, the number of samples (142) of real traffic data is very low and the algorithm performance should be correctly assessed on a much larger and more varied dataset in order to make more precise quantitative statements.

ACKNOWLEDGEMENTS

Financial support from *Gunnar och Märtha Bergendahls Stiftelse*, GEVEKO AB and the Swedish Governmental Agency for Innovation Systems (VINNOVA) are hereby gratefully acknowledged.

REFERENCES

- Andrieu, C., de Freitas, N., Doucet, A., and Jordan, M.I. (2003). An introduction to MCMC for machine learning. *Machine Learning*, 50, 5–43.
- Birk, W., Osipov, E., and Eliasson, J. (2009). iRoad – cooperative road infrastructure systems for driver support. In *16th ITS World Congress 2009, Stockholm Sweden*.
- Cheung, S.Y. and Varaiya, P. (2007). Traffic surveillance by wireless sensor networks: Final report. Technical report, California Path Program, Institute of Transportation Studies, University of California, Berkeley.
- Ding, J., Cheung, S.Y., Tan, C.W., and Varaiya, P. (2004). Signal processing of sensor node data for vehicle detection. 70–75.

- Federal Highway Administration (2006). Traffic detector handbook. Technical report, Federal Highway Administration.
- Hao, H. and Ang, T.C. (1998). Analytical modeling of traffic-induced ground vibrations. *Journal of Engineering Mechanics*, 124(8), 921–928.
- Honeywell (2005). Vehicle detection using AMR sensors. Technical report, Honeywell International Inc.
- Hostettler, R. and Birk, W. (2011). Analysis of the adaptive threshold vehicle detection algorithm applied to traffic vibrations. In *18th IFAC World Congress*. Milano, Italy.
- Hostettler, R., Birk, W., and Lundberg Nordenvaad, M. (2010). Feasibility of road vibrations-based vehicle property sensing. *Intelligent Transport Systems, IET*, 4(4), 356–364.
- Hunt, H.E.M. (1991). Stochastic modelling of traffic-induced ground vibration. *Journal of Sound and Vibration*, 144(1), 53 – 70.
- Isaksson, M. (2008). *Vehicle Detection using Anisotropic Magnetoresistors*. Master's thesis, Chalmers University of Technology.
- Papoulis, A. (1984). *Probability, Random Variables, and Stochastic Processes*. McGraw-Hill.
- SENSYS Networks (2010). Wireless vehicle detection systems. Company Website. URL <http://www.sensysnetworks.com>.
- Sullivan, J.M., Winkler, C.B., and Hagan, M.R. (2005). Smart barrel for an adaptive queue-warning system. Technical report, University of Michigan.
- Sun, L. and Kennedy, T.W. (2002). Spectral analysis and parametric study of stochastic pavement loads. *Journal of Engineering Mechanics*, 128(3), 318–327.
- Triggs, T.J. and Harris, W.G. (1982). Reaction time of drivers to road stimuli. Technical report, Monash University.
- Wahlström, N., Callmer, J., and Gustafsson, F. (2010). Magnetometers for tracking metallic targets. In *Proceedings of 13th International Conference on Information Fusion*. Edinburgh, Scotland.

Appendix A. DERIVATIONS

A.1 Signal Characteristics for Hypothesis H_0

Signal The input signal for when H_0 is present is given in (1). This yields the output signal

$$y^{(0)}[n] = g_2 * (g_1[n] * e[n])^2 \quad (\text{A.1})$$

where $*$ denotes the convolution. Based on that, the output mean and variance can be determined in order to characterize the output statistics.

Output Mean Since the input is a zero mean Gaussian random process with static non-linearity, the output mean is given by

$$\begin{aligned}
\eta_y^{(0)} &= E \left\{ y^{(0)}[n] \right\} \\
&= E \left\{ g_2[n] * (g_1[n] * e[n])^2 \right\} \\
&= g_2[n] * E \left\{ (g_1[n] * e[n])^2 \right\} \\
&= G_2(0)E \left\{ (g_1[n] * e[n])^2 \right\}.
\end{aligned}$$

The mean output $E \left\{ (g_1[n] * e[n])^2 \right\}$ of the squarer is equal to the variance of the pre-filtered input. Given the assumption of ideal filters, this is

$$E \left\{ (g_1[n] * e[n])^2 \right\} = \frac{\sigma^2}{\pi} (\omega_u - \omega_l).$$

And therefore, the output mean becomes

$$\eta_y^{(0)} = \frac{\sigma^2}{\pi} (\omega_u - \omega_l). \quad (\text{A.2})$$

Output Variance The output variance is calculated using the output autocorrelation. The input autocorrelation is given as $R_{xx}^{(0)}[k] = R_{ee}[k] = \sigma^2 \delta[k]$ which has the power spectral density $S_{xx}^{(0)}(\omega) = \sigma^2$. Applying the pre-processing as described in Section 3.1 yields the output power spectral density

$$\begin{aligned}
S_{yy}^{(0)}(\omega) &= \eta_y^{(0)2} \delta(\omega) + \frac{\sigma^4}{\pi} \left(2(\omega_u - \omega_l - \omega_c) \text{rect} \left(\frac{\omega}{2\omega_c} \right) \right. \\
&\quad \left. - 2|\omega| + |\omega + \omega_c| + |\omega - \omega_c| \right).
\end{aligned} \quad (\text{A.3})$$

Taking the inverse Fourier transform yields

$$\begin{aligned}
R_{yy}^{(0)}[k] &= \eta_y^{(0)2} + \frac{2\sigma^4}{\pi^2} \left(\omega_c(\omega_u - \omega_l - \omega_c) \text{sinc} \left(\frac{\omega_c}{\pi} k \right) \right. \\
&\quad \left. + 2 \left(\frac{\omega_c}{2} \text{sinc} \left(\frac{\omega_c}{2\pi} k \right) \right)^2 \right)
\end{aligned} \quad (\text{A.4})$$

for the output autocorrelation function. The output variance is now calculated by

$$\sigma_y^{(0)2} = R_{yy}^{(0)}[0] - \eta_y^{(0)2} \quad (\text{A.5})$$

and the output distribution is approximated as a $\Gamma(\alpha, \beta)$ distribution since it is a (weighted) sum of squared Gaussian random variables. The parameters α and β are

$$\alpha = \frac{\eta_y^{(0)2}}{\sigma_y^{(0)2}}, \quad \beta = \frac{\sigma_y^{(0)2}}{\eta_y^{(0)}}. \quad (\text{A.6})$$

Note that the output is wide sense stationary since $\eta_y^{(0)}$ is constant and $R_{yy}^{(0)}[k]$ is a function of the time difference k .

A.2 Signal Characteristics for Hypothesis H_1

Signal For H_1 , the input signal is a superposition of signal and noise as described in (2). This input signal yields the output

$$\begin{aligned}
y^{(1)}[n] &= g_2[n] * ((g_1[n] * s[n])^2 \\
&\quad + 2(g_1[n] * s[n])(g_1[n] * e[n]) \\
&\quad + (g_1[n] * e[n])^2).
\end{aligned}$$

Since $s[n]$ is bandlimited within (ω_l, ω_u) , the filtering $g_1[n] * s[n] = s[n]$. Furthermore, the output of the squared, post-filtered signal is $g_2[n] * s^2[n] = \frac{A^2}{2} p^2[n]$ since $\omega_b < \omega_c$. This yields

$$\begin{aligned}
y^{(1)}[n] &= \frac{A^2}{2} p^2[n] + 2g_2[n] * (s[n](g_1[n] * e[n]) \\
&\quad + (g_1[n] * e[n])^2).
\end{aligned} \quad (\text{A.7})$$

We note that the output consists of the (desired), filtered signal as well as the filtered noise component as shown earlier. Additionally, a new noise-like component is generated (by the squarer) which is a cross product of the signal and the input noise.

Output Mean The output mean is the expected value of the output signal shown in (A.7). It can be easily shown that the middle term has an expected value of 0. The output mean therefore becomes the sum of the filtered signal and the output mean $\eta_y^{(0)}$ of the noise-only case

$$\eta_y^{(1)}[n] = \frac{A^2}{2} p^2[n] + \eta_y^{(0)} = \frac{A^2}{2} p^2[n] + \frac{\sigma^2}{\pi} (\omega_u - \omega_l). \quad (\text{A.8})$$

Output Variance The output variance is calculated by using the second order moment and the mean (Papoulis, 1984, pp. 108):

$$\sigma_y^{(1)2}[n] = E \left\{ y^{(1)2}[n] \right\} - E \left\{ y^{(1)}[n] \right\}^2 \quad (\text{A.9})$$

Using (A.7) in (A.9) and simplifying it, it can be shown that

$$\sigma_y^{(1)2}[n] = E \left\{ (2g_2[n] * (s[n](g_1[n] * e[n]))^2 \right\} + \sigma_y^{(0)2},$$

i.e. the sum of the output variance of the mixed term and the output variance of the noise. The latter is given in (A.5). For the first part, it can be shown that

$$E \left\{ (g_2[n] * (s[n](g_1[n] * e[n]))^2 \right\} = 2A^2 p^2[n] \frac{\sigma^2}{\pi^2} \omega_c (\omega_u - \omega_l)$$

and the variance becomes

$$\sigma_y^{(1)2}[n] = 8A^2 p^2[n] \frac{\sigma^2}{\pi^2} \omega_c (\omega_u - \omega_l) + \sigma_y^{(0)2}. \quad (\text{A.10})$$

Note that the output mean as well as the variance vary with time and the output is no longer wide sense stationary. Again, the output is approximated by a Γ -distribution with parameters as described by (A.6) but using $\sigma_y^{(1)2}$ and $\eta_y^{(1)}$ instead.